Title
Remotely controlled chemomagnetic modulation of targeted neural circuits

Authors
Rao, Siyuan
Chen, Ritchie
LaRocca, Ava A
et al.

Peer reviewed

Remotely Controlled Chemomagnetic Modulation of Targeted Neural Circuits

Siyuan Rao[1,2], **Ritchie Chen**[2,6], **Ava A. LaRocca**[3], **Michael G. Christiansen**[1,3,7], **Alexander W. Senko**[1,3], **Cindy H. Shi**[3], **Po-Han Chiang**[1], **Georgios Varnavides**[1,3], **Jian Xue**[4,5], **Yang Zhou**[4,5], **Seongjun Park**[1,8], **Ruihua Ding**[9,10], **Junsang Moon**, **Guoping Feng**[1,3,4,5], **Polina Anikeeva**[1,3,4,5,*]

[1]Research Laboratory of Electronics, Massachusetts Institute of Technology, Cambridge, MA 02139, USA. [2]Simons Center for Social Brain, Massachusetts Institute of Technology, Cambridge, MA 02139, USA. [3]Department of Materials Science and Engineering, Massachusetts Institute of Technology, Cambridge, MA 02139, USA. [4]McGovern Institute for Brain Research, Massachusetts Institute of Technology, Cambridge, MA 02139, USA. [5]Department of Brain & Cognitive Sciences, Massachusetts Institute of Technology, Cambridge, MA 02139, USA. [6]Department of Bioengineering, Stanford University, Stanford, CA 94305, USA. [7]Department of Health Sciences and Technology at the Swiss Federal Institute of Technology in Zürich (ETHZ), Zürich 8093, Switzerland. [8]Department of Electrical Engineering and Computer Science, Massachusetts Institute of Technology, Cambridge, MA 02139, USA. [9]John A. Paulson School of Engineering and Applied Sciences, Harvard University, Cambridge, MA 02138, USA. [10]Department of Chemistry and Chemical Biology, Harvard University, Cambridge, MA 02138, USA.

Abstract

Connecting neural circuit output to behaviour can be facilitated by precise chemical manipulation of specific cell populations[1,2]. Engineered receptors exclusively activated by designer small molecules enable manipulation of specific neural pathways[3,4]. Their application to studies of behaviour has thus far been hampered by a trade-off between low temporal resolution of systemic injection versus invasiveness of implanted cannulas or infusion pumps[2]. Here, we develop remotely controlled chemomagnetic modulation – a nanomaterials-based technique that permits pharmacological interrogation of targeted neural populations in freely moving subjects. The heat

*All questions and requests for samples should be addressed to: anikeeva@mit.edu.

dissipated by magnetic nanoparticles in the presence of alternating magnetic fields triggers small molecule release from thermally sensitive lipid vesicles with 20 s latency. Coupled with chemogenetic activation of engineered receptors, this technique permits the control of specific neurons with temporal and spatial precision. Delivery of chemomagnetic particles to the ventral tegmental area allows remote modulation of motivated behaviour in mice. Furthermore, this chemomagnetic approach activates endogenous circuits by enabling regulated release of receptor ligands. Applied to an endogenous dopamine receptor D1 agonist in the nucleus accumbens, a brain area involved in mediating social interactions, chemomagnetic modulation increases sociability in mice. By offering temporally precise control of specified ligand-receptor interactions in neurons, this approach may facilitate molecular neuroscience studies in behaving organisms.

Local delivery of neuromodulators within the brain allows for linking of their molecular targets to behavior[5]. Systemic delivery of compounds via intravenous or intraperitoneal injection does not permit localized chemical neuromodulation and may be accompanied by off-target effects, while efficacy is further impeded by the limited blood-brain barrier permeability[6]. Consequently, permanently implanted cannulas are typically used for local delivery of compounds to the neural circuits of interest[7]. To facilitate spatially restricted and remotely controlled delivery of neuromodulators to neural targets, we sought to gate the release of small molecules using non-invasive stimuli. We applied weak alternating magnetic fields (AMFs) with frequencies of hundreds of kilohertz, that can access arbitrarily deep tissue volumes[8,9] to produce hysteretic heating by magnetic nanoparticles (MNPs). MNP heating in AMFs has been extensively applied in cancer hyperthermia[10], and has been recently leveraged to control cellular signaling[8,11], gene expression[12], and mouse behaviour by triggering heat-sensitive ion channels[13]. Here, we apply AMF stimulation to remotely control the release of chemical compounds from thermally-sensitive liposomes loaded with MNPs. Multiple micro-doses could be delivered through liposome permeabilization upon localized AMF-triggered heating of MNPs, while negligible leakage was observed in the absence of an AMF. When combined with the chemogenetic neuromodulation approach, designer receptors exclusively activated by designer drugs (DREADDs)[4,14], this method decreases response time from hours to tens of seconds at multiple time points within genetically-defined neural populations. This scheme is further generalized to endogenous circuits by enabling local delivery of receptor agonists and antagonists, thus facilitating the dissection of behaviour by activating ligand-receptor pairs.

We designed a chemomagnetic gate consisting of thermally responsive (MNP-loaded) liposomes composed of a mixture of 1,2-dipalmitoyl-sn-glycero-3-phosphocholine (DPPC), 1,2-distearoyl-sn-glycero-3-phosphocholine (DSPC) lipids and cholesterol, (10:5:3 weight ratio)[15,16] with a phase transition temperature of 43 °C (Fig. 1a). To synthesize magnetic liposomes loaded with chemical neuromodulators, we used a double-emulsion method[15] (Supplementary Fig. 1). In brief, MNPs and the payload were solubilized in an aqueous phase, and then transferred into a solution of amphiphilic lipids in a hydrophobic solvent. Following homogenization, the aqueous phase containing MNPs and the payload was encapsulated within the lipid micelles, and rapid evaporation of the hydrophobic phase produced double-micelle magnetoliposomes with diameters of 426±346 nm (Fig. 1b). The magnetoliposomes maintained structural integrity following 40 s exposure to AMF ($H_0 =$

45 ± 2 mT, $f=150$ kHz), indicating their stability across multiple release cycles (Fig. 1b). As latency of release following AMF application scales inversely with the MNP heating efficiency (specific loss power), for physiologically safe AMFs with a frequency $f=150$ kHz and amplitudes H_0 60 mT[17], 25 nm iron oxide MNPs were selected[18]. Their specific loss power values were calorimetrically measured (741 ± 30 W/g$_{[Fe]}$, $H_0=45\pm2$ mT, $f=150$ kHz) using a custom AMF coil driven by a resonant circuit (Supplementary Fig. 2)[19]. Using fluorescent dye as a 'payload', minimal background leakage from the liposomes was observed at 37 °C. Gradual release was observed when the temperature exceeded the lipid phase transition point of 43 °C (Fig. 1c). Release of the payload due to the local MNP heating within the magnetoliposomes scaled with the duration of the AMF stimulus, while only negligible increase in bulk solution temperature was observed (Fig. 1d).

Chemomagnetic modulation of cell function was first evaluated *in vitro*. Due to their minimal cross-reactivity with endogenous receptors, DREADDs have become indispensable tools for chemogenetic neuromodulation[3,14]. We therefore selected DREADDs as targets for chemomagnetic control of intracellular calcium (Ca^{2+}) in rat primary hippocampal neurons (Fig. 1e–i) and human embryonic kidney (HEK293FT) cells (Supplementary Fig. 3). Hippocampal cells were either transduced with an adeno-associated virus serotype 9 (AAV9) carrying a depolarizing DREADD hM3D(Gq), commonly used for chemogenetic neural excitation[3], fused to a red fluorescent protein mCherry (*AAV9-hSyn::hM3D(Gq)-mCherry*, hM3D(Gq)$^+$) or with an AAV9 carrying a fluorophore alone (*AAV9-hSyn::mCherry*, hM3D(Gq)$^-$). The cells were also transduced with an AAV9 carrying a fluorescent calcium indicator, GCaMP6s (*hSyn::GCaMP6s*), to record intracellular Ca^{2+} changes as a proxy for membrane depolarization (Fig. 1e)[20]. GCaMP6s and hM3D(Gq) expression and function were first corroborated by fluorescence imaging of Ca^{2+} influx in response to the hM3D(Gq) ligand clozapine N-oxide (CNO) (Supplementary Fig. 4). By applying AMF in the presence of magnetoliposomes encapsulating CNO, over 60% of hM3D(Gq)$^+$ neurons exhibited synchronized firing after the stimulus (Fig. 1f and Supplementary Fig. 5), whereas only sporadic activity was observed in hM3D(Gq)$^-$ neurons (or in the absence of stimuli) (Fig. 1 g–i). This implies that the CNO release from the magnetoliposomes in the presence of the AMF was necessary and sufficient to trigger hM3D(Gq) and cause membrane depolarization in neurons while avoiding nonspecific thermal effects. The latter was corroborated by the chemomagnetic stimulation of HEK293 cells expressing the heat-sensitive transient receptor potential cation channel subfamily V member 1 (TRPV1) (*CamKIIa::TRPV1-p2A-mCherry*) that did not show significant response to AMF in the presence of magnetoliposomes (Supplementary Fig. 6). Analogous experimental scheme has also been implemented with neurons expressing inhibitory DREADD hM4D(Gi), and neural inhibition was observed following AMF stimulation in the presence of CNO-loaded magnetoliposomes, indicating future opportunities in bi-directional control (Supplementary Fig. 7).

We next tested the chemomagnetic neural excitation approach in the mouse ventral tegmental area (VTA), a deep brain structure. The VTA, and its projection circuits, have been extensively researched in the context of motivated and social behaviors[21], reward processing[22], substance abuse[23], and depression[24], making this region a robust and biologically important target of neuromodulation techniques[25]. Broad expression of

hM3D(Gq)-mCherry in VTA neurons was observed following AAV delivery (AAV5-*hSyn::hM3D(Gq)-mCherry* or AAV5-*hSyn::mCherry*) (Fig. 2a). Following an incubation period of 5–6 weeks, magnetoliposomes were injected into the same region (Fig. 2a), and the anesthetized mice were transferred into a custom coil with $\pi \times 3.5 \times 3.5 \times 5$ cm^3 working volume[19], and subjected to a sequence of 5 AMF cycles (f=164 kHz and H_0 = 45±2 mT) with 40 s ON epochs, followed by 40 s OFF rest periods (Supplementary Fig. 8). To predict the payload distribution after AMF stimulation, we used an Abaqus drug diffusion model quantifying the CNO concentration. We found that 1 μl injection of CNO-loaded magnetoliposomes was sufficient to activate hM3D(Gq) across the entire VTA following 40 s AMF stimulus and a 5 min diffusion period (Supplementary Fig. 9). Bulk heating was not observed during AMF stimulation for the identical volume and concentration of magnetoliposomes solution injected into a brain phantom (0.6% agarose gel) (Supplementary Fig. 10).

Immunofluorescence analysis of the expression of c-fos, an immediate early gene and a marker of neural activity[26], revealed that neuronal excitation in the VTA was only triggered by the AMF in mice expressing hM3D(Gq) and injected with CNO-loaded magnetoliposomes (Fig. 2b). Consistent with other neuromodulation techniques[8,21], neural activity in the VTA resulted in the upregulated c-fos expression in the downstream excitatory projection targets, the nucleus accumbens (NAc) and medial prefrontal cortex (mPFC) (Fig. 2c–d). CNO-loaded magnetoliposomes remained effective for upregulating c-fos expression up to 7 days following injection (Supplementary Fig. 11–12).

Neuronal excitation in response to AMF-triggered release of CNO in the VTA was also photometrically recorded as a Ca^{2+}-dependent increase in GCaMP6s fluorescence in mice freely moving within the AMF coil (Fig. 2e). Neurons in the VTA were transduced with an AAV9 cocktail containing *hSyn::hM3D(Gq)-mCherry* (or a control plasmid *hSyn::mCherry*) and *hSyn::GCaMP6s* (Fig. 2f). A 5–6 week incubation period was followed by a magnetoliposome injection and optical fibre implantation. Consistent with the *in vitro* evaluation and c-fos expression, AMF robustly evoked Ca^{2+} influx, as measured by GCaMP6s fluorescence, in the VTA of mice expressing hM3D(Gq) and injected with magnetoliposomes containing CNO. No significant Ca^{2+} influx was found in mice expressing the Ca^{2+} indicator alone or injected with magnetoliposomes lacking the CNO payload (Fig. 2g).

Given the cellular effects observed in the VTA, we next tested whether chemomagnetic stimulation could shape behaviour in freely moving mice. As neural activity in the VTA is correlated with motivated behaviors[24], we hypothesized that mouse mobility in a forced swim test (FST) would be affected by the chemomagnetic stimulation. Akin to c-fos quantification experiments described above, VTA neurons were transfected to express *hM3D(Gq)-mCherry* or *mCherry* alone under the *hSyn* promoter, and the magnetoliposomes were delivered following an incubation period of 5–6 weeks. Three days following recovery from the latter injection surgery, the mice were subjected to a 6 min FST assay (Fig. 3) in a container placed within the AMF coil (Fig. 3a and Supplementary Fig. 13). The water level was set to position the VTA in the central area of the coil to ensure uniform AMF amplitude during the entire stimulation epoch (Fig. 3b). It has been shown that repeated exposure of

mice to the FST induces adaptation manifested as reduced baseline mobility[27]. To capture the dynamic range of the behavioural responses to the applied AMF, we developed a classifier for unbiased automated selection of mice that exhibited such adaptation behaviour (Fig. 3c). The classifier fitted a linear combination of Gaussian distributions to the mobility data, and mice classified as belonging to a mobility distribution centred around 0% prior to AMF exposure were considered to have adapted (Fig. 3c). The mobility of the adapted mice was significantly enhanced by the CNO release in the VTA triggered during the 40 s AMF exposure, and the effect was conditional on hM3D(Gq) expression (Fig. 3d–e). In the absence of hM3D(Gq) expression, CNO loading in the magnetoliposomes, or AMF exposure, mobility did not vary significantly within the experimental trials. To determine the period of efficacy of the CNO release from the magnetoliposomes, we subjected the same cohort of adapted hM3D(Gq)$^+$ mice to the FST assay for 3 consecutive days. We repeatedly observed increased mobility in response to chemomagnetic stimulation (Fig. 3f), consistent with the stable on-demand release profiles found for the magnetoliposomes in cell cultures.

As the chemomagnetic approach is largely independent of the chemistry of water-soluble payloads, we sought to extend it to modulation of non-modified, genetically intact neural circuits. Optogenetic excitation of VTA projections to the NAc was previously shown to enhance social interactions in mice, and the effect could be blocked by the dopamine receptor D1 (DRD1) antagonist SCH-23390[21]. Based on this evidence, we reasoned that chemomagnetic release of a DRD1 agonist or antagonist in the NAc should influence social behavior[28]. To test this hypothesis, the DRD1 agonist SKF-38393, DRD1 antagonist SCH-23390, or saline were loaded into the magnetoliposomes, and then injected into the NAc of wild-type mice. Another group of wild-type mice that did not receive any material injection was set as naïve group to investigate the potential influence of AMF alone on social behaviour. A social preference assay compatible with chemomagnetic modulation was developed by constructing an AMF stimulation chamber connecting two test chambers that housed either a novel object or a novel mouse (Fig. 4a and Supplementary Fig. 14). Prior to the social preference assay, we confirmed that the mice did not exhibit a preference bias for either of the test chambers (Supplementary Fig. 15). During the social preference assay, the test mice were first confined to the stimulation chamber for 1 min of habituation and then exposed to 40 s of AMF. The mice were then released from the stimulation chamber to freely explore the two adjacent test chambers for 5 min. No significant differences in locomotor performance among agonist, antagonist and saline groups were observed (Supplementary Fig. 16). Consistent with activation of DRD1-expressing neurons in the NAc, only the mice injected with the DRD1 agonist-loaded magnetoliposomes displayed an increased social preference following AMF stimulation (Fig. 4b–c and Supplementary Fig. 17). The ability of the magnetoliposomes to release multiple doses of their payloads has enabled repeated control of sociability in the DRD1 agonist group, albeit the significance of the effect was reduced to a trend on the third day of exposure (Fig. 4d).

To evaluate the biocompatibility and stability of the magnetoliposomes *in vivo*, we examined the interface between these particles and the tissue. Four weeks following injection, magnetoliposomes were observable (Supplementary Fig. 18), but did not cause significant glial activation and macrophage accumulation (Supplementary Fig. 19). The minimal foreign body reaction by surrounding tissues may in part be attributed to the lipid-based

chemistry of the magnetoliposomes[29], and clinically assessed biochemical inertness of iron oxide nanoparticles[30]. No significant cytotoxicity was observed following AMF stimulation neither *in vitro* (Supplementary Fig. 20) nor *in vivo* (Supplementary Fig. 21), consistent with the material inertness and negligible thermal effects of chemomagnetic stimulation.

We designed a chemomagnetic strategy that affords spatially targeted and temporally precise molecular control of neural circuits by coupling a non-invasive magnetic field cue with magnetically responsive liposomal drug carriers. Magnetically gated small molecule release facilitated fast activation of both genetically engineered and endogenously expressed receptors within targeted neural populations during behavioural experiments. The chemomagnetic paradigm may in future be multiplexed to various ligand-receptor pairs enabling remote modulation of multiple cell populations and permitting studies of drug interactions in behaving subjects[17].

Materials and Methods

Molecular cloning and virus packing

For the construction of *pLenti-CamKIIα-hM3D(Gq)-p2A-mCherry*, we first obtained the hM3D(Gq) fragment from *pAAV-CaMKIIα-hM3D(Gq)-mCherry* (a gift from Bryan Roth, Addgene plasmid # 50476) by PCR with primers 5'-GGGCAGCGGGGGATCCGCCACCATGACCTTGCACAATAAC-3' and 5'-GGAGCCGGGCGCGCCTTTCAAGGCCTGCTCGGGTG-3'. The linearized vector was obtained from *pLenti-CamKIIα-TRPV1-p2A-mCherry* (developed in house)[1] by PCR with primers 5'- GGATCCCCCGCTGCCCC-3' and 5'- GGCGCGCCCGGCTCC-3'. The hM3D(Gq) was cloned into the p2A construct, replacing TRPV1. *pAAV-hSyn-hM3D(Gq)-mCherry* was a gift from Bryan Roth (Addgene plasmid # 50474 and Addgene viral prep # 50474-AAV5). *pGP-CMV-GCaMP6s* was a gift from Douglas Kim (Addgene plasmid # 40753). AAV5-*hSyn-mCherry* and AAV9-*hSyn-hM3D(Gq)-mCherry* were prepared by Boston Children's Hospital viral core. *pAAV-hSyn-GCaMP6s-WPRE-SV40* was a gift from The Genetically Encoded Neuronal Indicator and Effector Project (GENIE) & Douglas Kim (Addgene viral prep # 100843-AAV9) AAV9-*hSyn::GCaMP6s*. Prior to use, all viral vectors were diluted to a titer of 10^{12} transducing units per mL.

Magnetoliposome preparation

25 nm amine-terminated iron oxide magnetic nanoparticles (MNPs, Ocean Nano Tech, SHA 25)[2], 1,2-dipalmitoyl-sn-glycero-3-phosphocholine (DPPC, Avanti Polar Lipids, 850355), 1,2-distearoyl-sn-glycero-3-phosphocholine (DSPC, Avanti Polar Lipids, 850365) and cholesterol (Sigma-Aldrich, C8667) were used for magnetoliposomes preparation. Lipids mixture was first dissolved in dichloromethane and the aqueous phase (MNPs with payloads) was added into lipid mixture. After homogenization (>6000 rpm), the second water phase solution was added followed by quick vortex mixing. Then evaporation was rapidly applied and kept for more than 30 min. For further purification, a magnetic separator was used (Ocean Nano Tech, SUPERMAG-01). The payload concentration and second water phase solution were summarized in Table 1.

Cell culture

Hippocampal culture was isolated from neonatal rat pups (P1) and dissociated with Papain (Worthington Biochemical). After physical trituration, dissociated neural cells were plated on 5 mm diameter glass slides in 24 well plates. The glass slides were cleaned by hydrochloric acid treatment, washed with sterile 70% ethanol in water, and then sterile water, and then coated with Matrigel (Corning). The cells were maintained in Neurobasal media (Invitrogen). Three days after seeding the cells, glial inhibition with 5-Fluoro-2'-deoxyuridine (FUDR, F0503 Sigma) was conducted, and then the culture was transfected with 1 μL AAV9 cocktail of *hSyn::GCaMP6s* and *hSyn::hM3D(Gq)-mCherry* or *hSyn::mCherry*. After a 5-day incubation period, calcium imaging experiments were performed on transfected cultures.

The HEK 293FT cell line was a gift by Feng Zhang (MIT) and maintained in DMEM (w GlutaMax)+10% Fetal Bovine Serum (FBS). To facilitate the imaging with alternating magnetic field (AMF) stimulation, the HEK cells were plated onto the Matrigel coated 5mm diameter glass slides in 24 well plates. Lipofectamine® 2000 was used for all transfections. We used 1 μL of Lipofectamine and 500 ng of DNA per 500 μL of media within each well.

In vivo studies

All experimental procedures were approved by the MIT Committee on Animal Care.

Adult male C57BL/6 mice (Jackson Laboratory) aged 8 weeks were used for c-fos quantification, behavioral assays, and fiber photometry experiments. Mice were group housed with the exception of those implanted with optical fibers, and were on a reverse 12 hr light/dark cycle with food and water ad libitum.

Virus and magnetoliposome injection, and optical fiber implantation

Mice were anaesthetized with isoflurane (0.5–2.5% in O_2) using a rodent anaesthesia machine (VET EQUIP) and positioned within a stereotaxic frame (David Kopf Instruments). During surgical procedures, ophthalmic ointment was applied to the eyes to prevent drying. All injections were conducted with a microinjection apparatus (10 μL Nanofil Syringe, beveled 34-gauge needles facing the dorso-lateral side, UMP-3 Syringe pump, and its controller Micro4, Word Precision Instruments) at an infusion rate of 100 nL/min. During the injections, the syringe was elevated by 100 μm from the initial coordinates. Following injections, the syringe needles remained inside the brain for another 10 min prior to slow withdrawal.

For c-fos quantification and forced swimming test (FST) assays, 300 nL of AAV5-*hSyn:: hM3D(Gq)-mCherry* or *hSyn::mCherry* with a titer of 10^{12} U/mL were injected bilaterally into the ventral tegmental area (VTA), with the coordinates relative to bregma according to Allen Mouse Brain Atlas: −3.08 mm anteroposterior (AP); ± 0.4 mm mediolateral (ML); −5 mm dorsoventral (DV). 1 μL of magnetoliposomes (~15 μg/ml) were also bilaterally injected into the same coordinates. For fiber photometry experiments, 600 nL AAV9 cocktail of *hSyn:: hM3D(Gq)-mCherry* or *hSyn::mcherry* and *hSyn::GCaMP6s* was injected unilaterally into the VTA, as well as 1 μL of magnetoliposomes. The optical fibres were

implanted a above the virally transduced volume with the coordinates: −3.08mm AP, +0.4mm or −0.4mm ML, −4.8mm DV. For social preference experiments, magnetoliposomes were bilaterally injected into the nucleus accumbens (NAc) (coordinates: +1.25mm AP, ± 0.75 mm ML, −4.5mm DV).

Following all injection surgeries the skin over the mouse skull was closed with sutures. During fibre implantation surgeries, the fibres were fixed onto the skull with multiple layers of adhesive (C&B Metabond, Parkell) and dental cement (Jet-set 4, Lang Dental). All mice were given a subcutaneous injection of buprenorphine (0.05 mg/kg) during surgery and warm Lactated Ringers solution during recovery.

Immunohistochemistry analysis

For c-fos quantification, mice were transfected with AAV5-*hSyn::hM3D(Gq)-mCherry* or *hSyn::mCherry* in the VTA, which was followed by 5–6 weeks incubation period followed by the magnetoliposomes injection into the same location. Following a recovery period of 3 days, mice were anesthetized *via* an intraperitoneal injection of ketamine (100 mg/kg) and xylazine (10 mg/kg) mixture and transferred to the magnetic coil for stimulation. The mice were subjected to a sequence of 5 AMF exposures (f =164 kHz and H_0 = 45±2 mT) with 40 s ON, followed by 40 s OFF, and then transferred back to their home cages for 90 min to allow for c-fos expression. The mice were then euthanized by a lethal intraperitoneal injection of a sodium pentobarbital (Fatal-plus; 390 mg/mL, dose 0.5 mg/g) followed by transcardial perfusion as described below.

For all immunohistochemistry studies, the mice were transcardially perfused with 4% paraformaldehyde (PFA) in phosphate buffered saline (PBS), and their brains were extracted and kept in 4 % PFA solution overnight at 4 °C. The fixed brain samples were then sectioned into 40 μm-thick coronal slices using a vibrating blade microtome (Leica VT1000S). The slices were permeabilized and blocked for 1 hour in dark at room temperature in 0.3 v/v% TritonX100 and 3 v/v % blocking serum solution in PBS in an orbital shaker. Following 3 washes with PBS, the brain slices were incubated in primary antibody solution (with 3% blocking serum) overnight at 4 °C. Following 3 washes with PBS, the brain slices were transferred into a secondary antibody solution and incubated in the dark for 3 hours at room temperature. Following another 3 washes with PBS, the brain slices were transferred onto glass slides, and mounted with mounting medium (VECTASHIELD containing DAPI nuclear stain). The primary antibodies, blocking serum, and secondary antibodies for c-fos quantification and biocompatibility analyses are summarized in Table 2.

Fibre photometry

In the fibre photometry setup, the 473 nm diode laser (OEM Laser Systems, 50 mW peak power) was controlled by a function generator (Agilent, 33500B Series, 400 Hz, square wave) and coupled to a 3 m long modified ferrule rotary joint patch cable with 400 μm core (Thorlabs, RJPFL4) using a 20X 0.45 NA microscope objective (Olympus) integrated with a fibre launch stage (Thorlabs, MBT610D). 400 μm 0.48 NA optical fibers (Thorlabs FP400URT) outfitted with ceramic ferrules (Thorlabs CF440–10) were implanted into mice and could be connected to the photometry patchcord linked to the fibre launch using a

ceramic split mating sleeves (Thorlabs ADAF1–5). The laser intensity out of the coupled fibre tip was set between 100–200 µW. The GCaMP6s fluorescence was collected by the same implanted optical fibre and transmitted through the objective and the dichroic mirror (Thorlabs, CM1-DCH). The collected fluorescence was then longpass filtered to eliminate any remaining laser background (Semrock, BLP01–473R-25) onto a femtowatt silicon photoreceiver (NewFocus 2151, Newport, AC High mode). The photoreceiver was directed connected to a lock-in amplifier (SR830 DSP, Stanford Research Systems, 8 ms time constant) and recorded by custom software written in LabView with acquisition frequency of 8.5 Hz. All fibre photometry experiments were performed during the dark phase of the light/dark cycle in the dark and the fibre patch cord was suspended above the magnetic coil to allow the mice to move freely during stimulation. The mice were acclimated to the photometry room for 1 hour and to the magnetic coil for 15 min prior to recording.

Behavioural assays

In all the behavioural experiments, adult male mice (C57BL/6, aged 8 weeks at the start of experimental procedures) were used during the dark phase of the light/dark cycle, and were acclimated to the behaviour room for 1 hr prior to testing. In the social preference assays, adult male mice (C57BL/6, aged 5–6 weeks) were used as strangers.

For the forced swimming test (FST) assay, a transparent plastic cylinder fitting into the magnetic field coil was used as a swimming tank. On Day 0, all mice were subjected to a 6-min pre-test swimming, and on the following 3 test days, each mouse experienced a 6-min swimming session each day. The first 180 s of the 6-min FST was set as the pre-stimulus epoch, then 40 s of AMF stimulation (or without AMF stimulation) was applied between 180s and-220s, defined as during-stimulus epoch, while the remaining 220–300 s was defined as a post-stimulus epoch. The water temperature was maintained at 28 °C. Mobility percentage was calculated as a ratio of the time that each mouse spent moving to the total time of each epoch.

For the social preference assay, two square chambers with dimensions 20 cm × 20 cm × 15 cm (L × W × H) were connected with a cylindrical tunnel surrounded by the magnetic field coil. Two gates were set at the entrances into the tunnel to confine the test mice to the stimulation chamber. During each trial, a test mouse was confined inside of the magnetic coil stimulation chamber for 1 min as habituation, and then exposed to 40 s of AMF stimulation (or without AMF stimulation). The gates were then lifted allowing the mouse to freely explore the two test chambers for 5 min. On Day 0, all test mice were subjected to this experimental paradigm in the absence of novel objects and social strangers in the chambers. During the following 3 days, each mouse was tested without AMF stimulation and with AMF stimulation on each day. The preference (social/neutral) was calculated as the ratio of the time spent in the social chamber (or in the social close interaction zone) to the time spent in the neutral chamber (or the neutral chamber close interaction zone) for each test mouse. In each trial, the locations of the new object and the stranger were counterbalanced, and a new stranger and object were presented. The central luminous power of each chamber was maintained at 180–190 lux (Grainger).

Analysis scripts

In FST experiments mouse movements were tracked using the Behavioral Monitoring Tool[5]. The mobility energy is calculated from the difference in pixel intensity of successive grayscale frames in the FST videos. Specifically, for each two successive frames the difference in grayscale intensity of each pixel is computed. If the absolute value of this difference is larger than a lower threshold, then the pixel difference is accumulated towards the total frame difference. This yields a one-dimensional array of total grayscale intensity changes. In order to get the final mobility energy we perform the following three operations: First, the intensity changes are normalized, to account for varying frame sizes. Then a low pass filter is applied to the array, to remove noise due to abrupt changes in light. Finally a moving average filter is applied, to obtain a smooth mobility energy curve. In the social preference experiments, the mice movements were tracked by ToxTrac[6,7] and the analysis was conducted using custom scripts written in Mathematica (Wolfram).

Data Availability Statement

The data that support the findings of this study are presented within the manuscript and are available from the corresponding author upon request.

Code Availability

All scripts are available from the corresponding author upon request.

Additional Information

Supplementary information is available in the online version of the paper. Reprints and permission information is available online at www.nature.com/reprints. Correspondence and requests for materials should be addressed to the corresponding author (P.A.).

Supplementary Material

Refer to Web version on PubMed Central for supplementary material.

Acknowledgments

References

References

1. Harris-Warrick RM & Marder E Modulation of neural networks for behavior. Annu. Rev. Neurosci 14, 39–57 (1991). [PubMed: 2031576]

2. Smith KS, Bucci DJ, Luikart BW & Mahler SV DREADDS: Use and application in behavioral neuroscience. Behav. Neurosci 130, 137 (2016). [PubMed: 26913540]

3. Sternson SM & Roth BL Chemogenetic tools to interrogate brain functions. Annu. Rev. Neurosci 37, 387–407 (2014). [PubMed: 25002280]

4. Urban DJ & Roth BL DREADDs (designer receptors exclusively activated by designer drugs): chemogenetic tools with therapeutic utility. Annu. Rev. Pharmacol. Toxicol 55, 399–417 (2015). [PubMed: 25292433]

5. Shields BC et al. Deconstructing behavioral neuropharmacology with cellular specificity. Science 356, eaaj2161 (2017). [PubMed: 28385956]

6. Misra A, Ganesh S, Shahiwala A & Shah SP Drug delivery to the central nervous system: a review. J. Pharm. Pharm. Sci 6, 252–273 (2003). [PubMed: 12935438]

7. Dagdeviren C et al. Miniaturized neural system for chronic, local intracerebral drug delivery. Sci. Transl. Med 10, eaan2742 (2018). [PubMed: 29367347]

8. Chen R, Romero G, Christiansen MG, Mohr A & Anikeeva P Wireless magnetothermal deep brain stimulation. Science 347, 1477–1480 (2015). [PubMed: 25765068]

9. Schuerle S, Dudani JS, Christiansen MG, Anikeeva P & Bhatia SN Magnetically actuated protease sensors for in vivo tumor profiling. Nano letters 16, 6303–6310 (2016). [PubMed: 27622711]

10. Pankhurst QA, Connolly J, Jones S & Dobson J Applications of magnetic nanoparticles in biomedicine. J. Phys. D Appl. Phys 36, R167 (2003).

11. Huang H, Delikanli S, Zeng H, Ferkey DM & Pralle A Remote control of ion channels and neurons through magnetic-field heating of nanoparticles. Nat. Nanotechnol 5, 602 (2010). [PubMed: 20581833]

12. Stanley SA et al. Radio-wave heating of iron oxide nanoparticles can regulate plasma glucose in mice. Science 336, 604–608 (2012). [PubMed: 22556257]

13. Munshi R et al. Magnetothermal genetic deep brain stimulation of motor behaviors in awake, freely moving mice. Elife 6, e27069 (2017). [PubMed: 28826470]

14. Roth BL DREADDs for neuroscientists. Neuron 89, 683–694 (2016). [PubMed: 26889809]

15. Yatvin MB, Weinstein JN, Dennis WH & Blumenthal R Design of liposomes for enhanced local release of drugs by hyperthermia. Science 202, 1290–1293 (1978). [PubMed: 364652]

16. Tai L-A et al. Thermosensitive liposomes entrapping iron oxide nanoparticles for controllable drug release. Nanotechnology 20, 135101 (2009). [PubMed: 19420485]

17. Christiansen MG, Senko A, Chen R, Romero G & Anikeeva P Magnetically multiplexed heating of single domain nanoparticles. Appl. Phys. Lett 104, 213103 (2014).

18. Romero G, Christiansen MG, Stocche Barbosa L, Garcia F & Anikeeva P Localized Excitation of Neural Activity via Rapid Magnetothermal Drug Release. Adv. Funct. Mater 26, 6471–6478 (2016).

19. Christiansen MG, Howe CM, Bono DC, Perreault DJ & Anikeeva P Practical methods for generating alternating magnetic fields for biomedical research. Rev. Sci. Instrum 88, 084301 (2017). [PubMed: 28863666]

20. Chen T-W et al. Ultrasensitive fluorescent proteins for imaging neuronal activity. Nature 499, 295 (2013). [PubMed: 23868258]

21. Gunaydin LA et al. Natural neural projection dynamics underlying social behavior. Cell 157, 1535–1551 (2014). [PubMed: 24949967]

22. Lammel S et al. Input-specific control of reward and aversion in the ventral tegmental area. Nature 491, 212 (2012). [PubMed: 23064228]

23. Nestler EJ Is there a common molecular pathway for addiction? Nat. Neurosci 8, 1445 (2005). [PubMed: 16251986]

24. Tye KM et al. Dopamine neurons modulate neural encoding and expression of depression-related behaviour. Nature 493, 537 (2013). [PubMed: 23235822]

25. Morales M & Margolis EB Ventral tegmental area: cellular heterogeneity, connectivity and behaviour. Nat. Rev. Neurosci 18, 73 (2017). [PubMed: 28053327]

26. Sagar S, Sharp F & Curran T Expression of c-fos protein in brain: metabolic mapping at the cellular level. Science 240, 1328–1331 (1988). [PubMed: 3131879]

27. Mul JD, Zheng J & Goodyear LJ Validity assessment of 5 day repeated forced-swim stress to model human depression in young-adult C57BL/6J and BALB/cJ mice. eNeuro 3, ENEURO. 0201–0216.2016 (2016).

28. Rahman S & McBride WJ D1–D2 dopamine receptor interaction within the nucleus accumbens mediates long-loop negative feedback to the ventral tegmental area (VTA). J. Neurochem 77, 1248–1255 (2001). [PubMed: 11389175]

29. Naahidi S et al. Biocompatibility of engineered nanoparticles for drug delivery. J Control Release 166, 182–194 (2013). [PubMed: 23262199]

30. Laurent S et al. Magnetic iron oxide nanoparticles: synthesis, stabilization, vectorization, physicochemical characterizations, and biological applications. Chem. Rev 108, 2064–2110 (2008). [PubMed: 18543879]

References for the Materials and Methods

1. Chen R, Romero G, Christiansen MG, Mohr A & Anikeeva P Wireless magnetothermal deep brain stimulation. Science 347, 1477–1480 (2015). [PubMed: 25765068]

2. Schuerle S, Dudani JS, Christiansen MG, Anikeeva P & Bhatia SN Magnetically actuated protease sensors for in vivo tumor profiling. Nano Lett 16, 6303–6310 (2016). [PubMed: 27622711]

3. Zhu X-N et al. Ephrin-B3 coordinates timed axon targeting and amygdala spinogenesis for innate fear behaviour. Nat. Commun 7, 11096 (2016). [PubMed: 27008987]

4. Park S et al. One-step optogenetics with multifunctional flexible polymer fibers. Nat. Neurosci 20, 612 (2017). [PubMed: 28218915]

5. http://ratmonitoring.sourceforge.net.

6. Rodriguez A et al. ToxTrac: a fast and robust software for tracking organisms. Methods Ecol. Evol 9, 460–464 (2018).

7. Rodriguez A, Zhang H, Klaminder J, Brodin T & Andersson M ToxId: an efficient algorithm to solve occlusions when tracking multiple animals. Sci. Rep 7, 14774 (2017). [PubMed: 29116122]
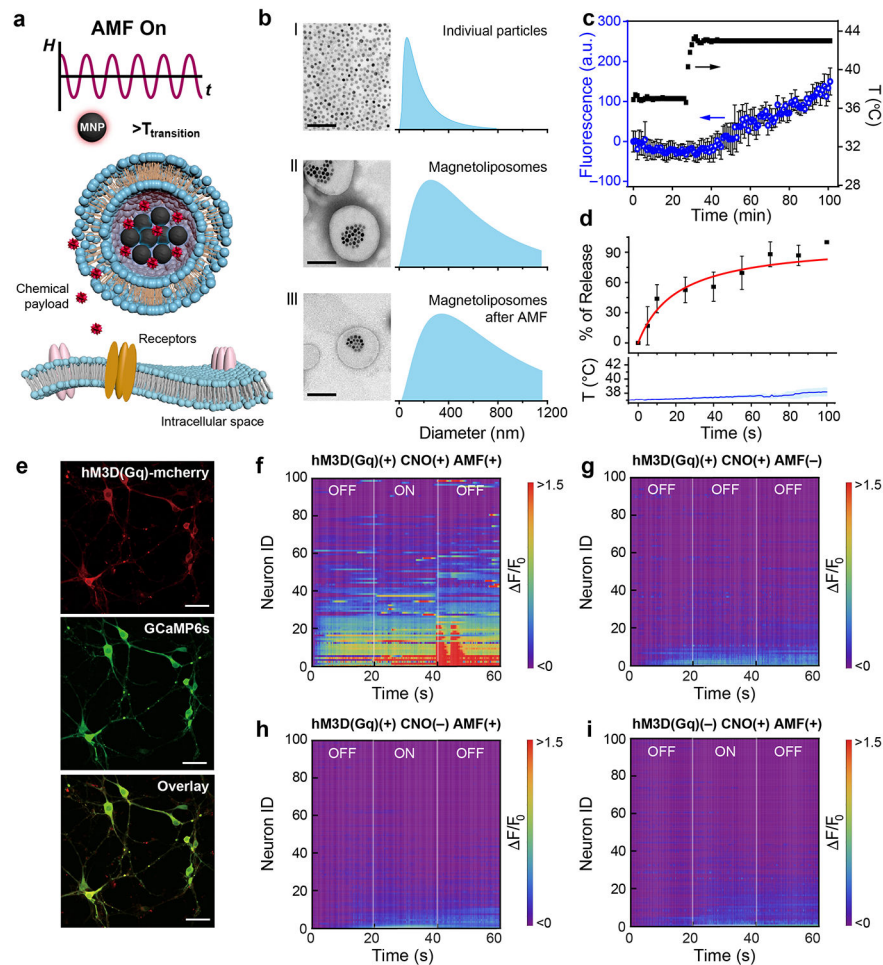
Figure 1. Magnetically controlled chemical payload release.
a, Experimental scheme of alternating magnetic field (AMF)-triggered chemical payload release from the magnetoliposomes. **b**, Transmission electron microscope (TEM) images and the size distributions from dynamic light scattering spectra of the magnetic nanoparticles (MNPs) before (I) and after (II) encapsulation into the magnetoliposomes, and the magnetoliposomes after exposure to 40 s of AMF (H_0=45±2 mT and f=150 kHz) (III). Scale bar: 200nm. **c**, Fluorescent dye (Alexa Fluor® 488) release from magnetoliposomes (mean ± standard deviation, s.d., n=3 independent samples) during the bath temperature increase from 37°C to 43°C. **d**, AMF-triggered dye release (mean ± s.d., n=3 independent samples) from magnetoliposomes and the temperature profile of the bulk solution (solid line: mean, shaded area: s.d. n=3). **e**, Confocal images of the primary hippocampal neurons expressing *hSyn::hM3D(Gq)-mCherry* and *hSyn-GCaMP6s*. Scale bar: 50μm. The experiment was repeated three times independently with similar results. **f-i**, Heat maps of normalized GCaMP6s fluorescence intensity of 100 automatically selected neurons in different experimental conditions. F_0 is defined as the mean of the fluorescence intensity during the first 10 s. ON: AMF is turned on. OFF: AMF is turned off. AMF conditions: H_0=45±2 mT, f=150 kHz, 20 s.
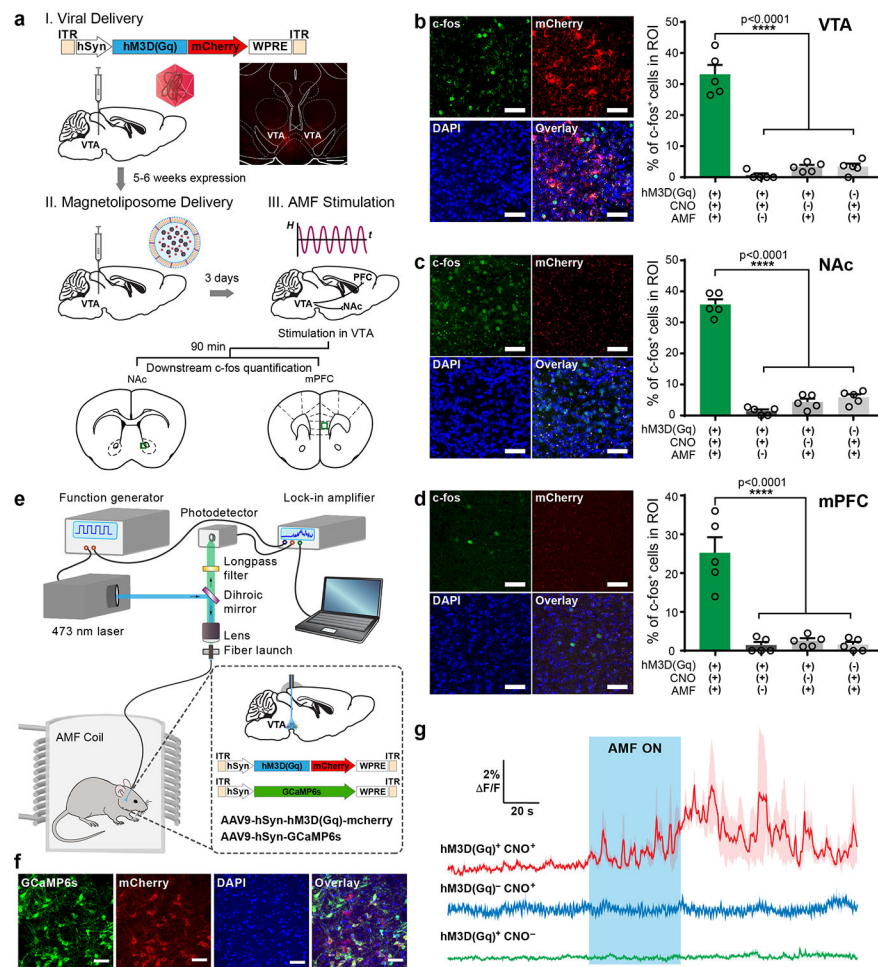
Figure 2. Chemomagnetic stimulation *in vivo*.

a, Experimental timeline for the viral gene delivery, magnetoliposome injection, and AMF stimulation. Inset: A confocal image of the expression of *hM3D(Gq)-mCherry* in the mouse VTA. Scale bar: 200 μm. **b-d**, Left: Confocal images of the c-fos expression in the VTA (**b**), NAc (**c**) and mPFC (**d**) of mice exposed to AMF (AMF[+]), injected with CNO-loaded magnetoliposomes (CNO[+]) and expressing hM3D(Gq) (hM3D(Gq)[+]). Scale bar: 50 μm. Right: the percentages of c-fos expressing (c-fos^{+}) neurons among DAPI-labelled cells in each group (mean ± standard error of the mean, s.e.m.). Increased c-fos expression is observed following chemomagnetic treatment as confirmed by one-way ANOVA and Turkey's multiple comparisons test (n=5 mice, VTA $F_{3,\ 16}$ = 86.29, NAc $F_{3,\ 16}$ = 207.6, mPFC $F_{3,\ 16}$ =30.97, **** $p<0.0001$). All c-fos quantification experiments were conducted in anesthetized mice. **e**, Photometry setup integrated with an AMF coil. **f**, Confocal images of co-expression of GCaMP6s and *hM3D(Gq)-mcherry* in the mouse VTA. The experiment was repeated three times independently with similar results. Scale bar: 50 μm. **g**, Normalized dynamic fluorescence intensity change (F/F$_0$) of GCaMP6s in the VTA of mice freely moving within the AMF coil. Fluorescence increase was observed only upon applying AMF stimulation in mice expressing hM3D(Gq) and injected with CNO-loaded magnetoliposomes (red). The blue area represents AMF exposure. In all experiments H_0

=45±2 mT, f = 164 kHz. Solid lines: mean, shaded areas: s.e.m., n=3 mice for each test condition.

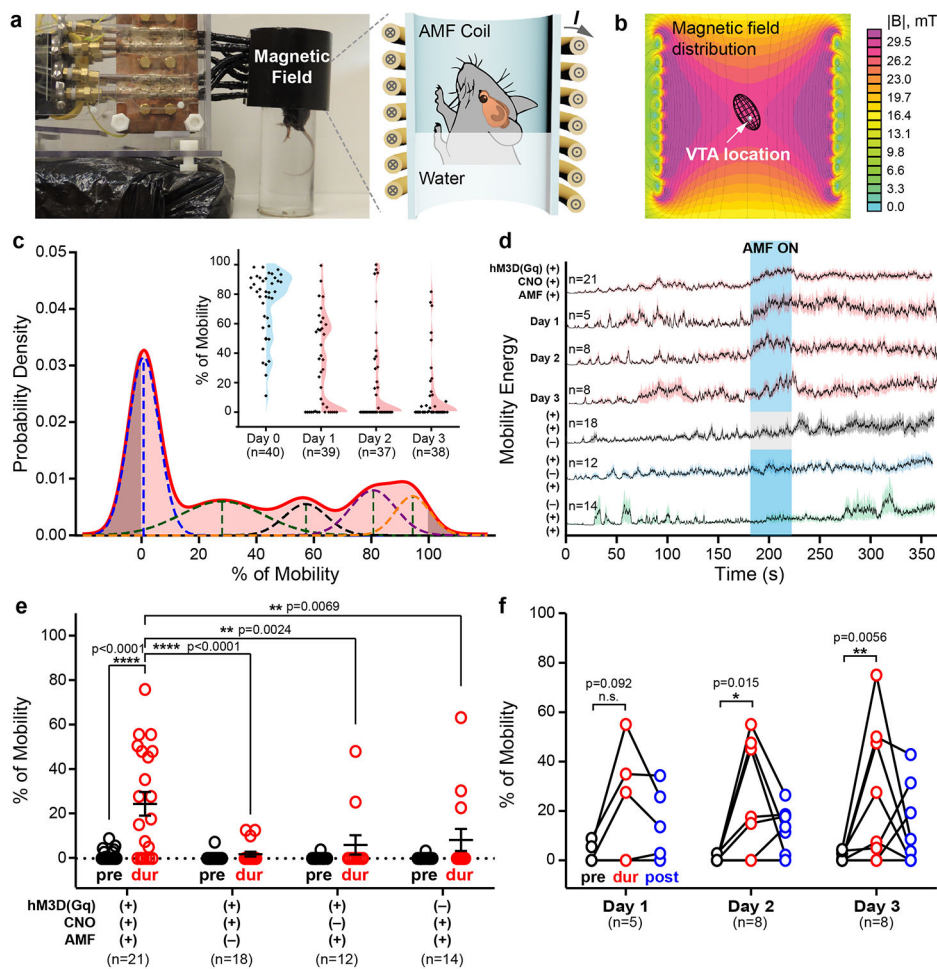**Figure 3. Remote chemomagnetic modulation of mouse behaviour using chemogenetics.**
a, A photograph and a schematic of the forced swimming test (FST) assay within an AMF coil. **b**, The mouse VTA was situated within the region of uniform AMF by adjusting the swimming tank water level. The color map represents the cross sectional view of the magnetic flux distribution as calculated by a finite element model for the AMF coil. **c**, Classification of mouse baseline mobility to identify adaptation in FST. Inset: the mobility percentage during the 6 min FST for all tested mice. The shaded areas display the Gaussian distribution of mouse mobility percentage on each day. Blue: training day, Day 0. Red: test days, Day 1–3. n represents the number of test trials. **d**, Averaged motion energy curves for mice undergoing FST. The energy is calculated from the pixel changes in each frame of the FST videos. Solid lines: mean, shaded areas: s.e.m. AMF conditions: H_0=45±2 mT, f = 164 kHz. The blue area represents AMF exposure, while the grey area indicates the absence of an AMF. n represents the number of subjects and test trials. **e**, Mice expressing hM3D(Gq) in the VTA neurons (hM3D(Gq)$^+$) and injected with CNO-loaded magnetoliposomes (CNO $^+$) exhibit enhanced swimming in response to the AMF stimulus (mean ± s.e.m., two-way ANOVA and Tukey's multiple comparisons test, $F_{3, 122}$ = 5.387, ** 0.001 p< 0.01, **** p<0.0001). pre: pre-stimulus epoch. dur: during AMF stimulation (or no AMF stimulation) epoch. post: post-stimulus epoch. Each marker represents an FST trial and n represents the
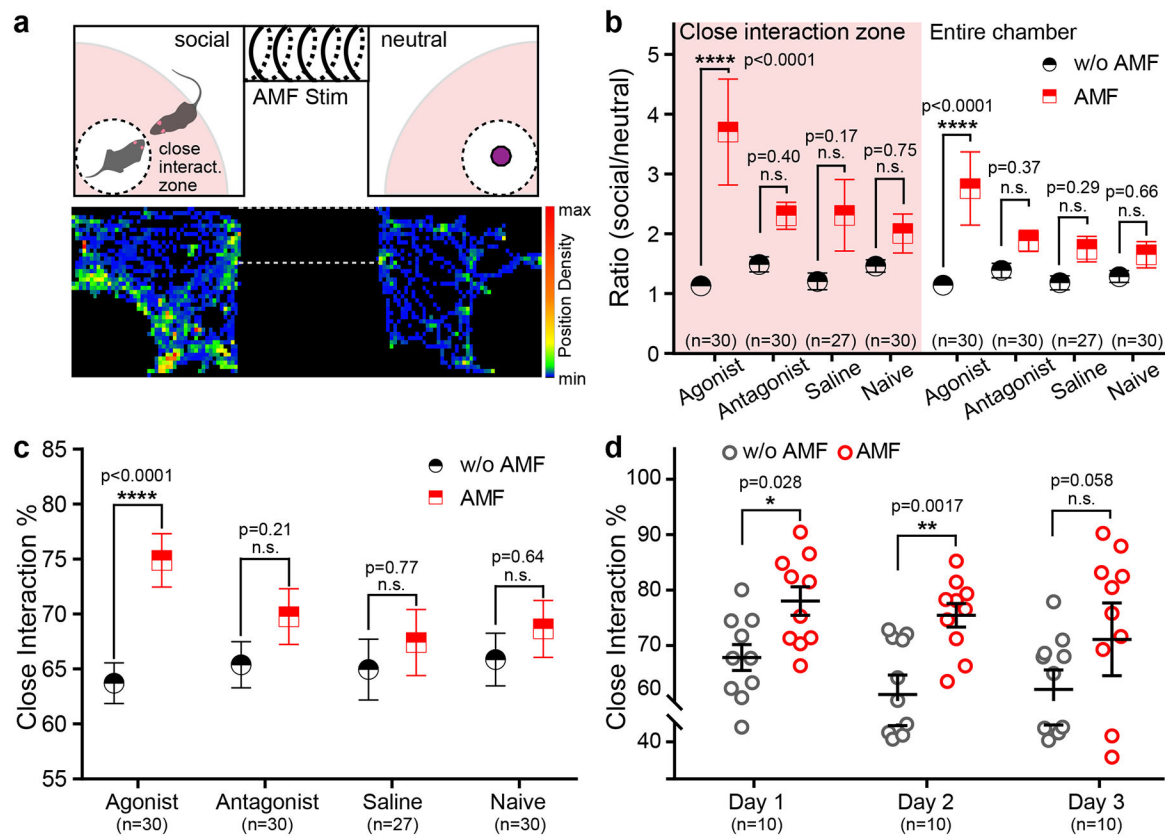
number of trials. **f**, Repeated enhancement of swimming behaviour is observed in hM3D(Gq)$^+$, CNO$^+$ group in response to AMF stimulation (two-way ANOVA and Tukey's multiple comparisons test, $F_{4, 36} = 0.05789$, n.s. p $\geq$ 0.05, * 0.01 $\leq$ p<0.05, ** 0.001 $\leq$ p<0.01). n represents the number of subjects and test trials.

Figure 4. Remote chemomagnetic modulation mediated by endogenous receptors.
a, Top: The experimental scheme for the mouse social preference test with an AMF coil encompassing the middle chamber. The shaded radial area within the test chambers (90% of the chamber length/width) was defined as the close interaction zone. Bottom: A representative heat map tracing the position of a mouse in social subject and novel object chambers during the preference test. **b**, The ratio of time spent in the social interaction chamber to the object (neutral) chamber is compared for mice subjected to AMF. The group with agonist-loaded magnetoliposomes exhibits enhanced social preference following exposure to AMF (mean ± s.e.m., two-way repeated measures ANOVA and Sidak's multiple comparisons test, close interaction $F_{3, 113}$= 3.053, entire chamber $F_{3,113}$=3.547, **** p<0.0001). n represents number of trials. **c**, The percentage of close interaction in the social chamber. The group injected with agonist-loaded magnetoliposomes spent more time in the close interaction zone (mean ± s.e.m., two-way repeated measures ANOVA and Sidak's multiple comparisons test, $F_{3, 113}$= 3.122, **** P<0.0001). n represents number of trials. **d**, The group injected with agonist-loaded magnetoliposomes repeatedly shows increased social preference following AMF exposure (mean ± s.e.m., two-way repeated measures ANOVA and Sidak's multiple comparisons test, $F_{2, 27}$= 0.5717, n.s. p $\geq$ 0.05, * 0.01 $\leq$ p< 0.05, ** 0.001 $\leq$ p< 0.01). n represents the number of subjects and test trials.

Table 1.

Payload concentration and second water phase solution

Payload	Initial concentration	Second water phase solution
Clozapine N-oxide (Tocris, 4936)	5 mg/mL	*In vitro*: Tyrode solution *In vivo*: Saline
SCH-23390 (Tocris, 0925)	2.5 mg/mL	Saline
SKF-38393 (Tocris, 0922)	2.5 mg/mL	Saline
Alexa Fluor 488 (Invitrogen)	100 μg/mL	Deionized water *In vivo*: Saline

Table 2.

Antibodies and blocking serum

Primary antibody	Blocking serum	Secondary antibody
Rabbit anti-cfos[3] (1:500, Cell Signaling technology, 2250s)	Normal Donkey Serum	Donkey anti-Rabbit, Alexa Fluor 488 (1:1000, Invitrogen, A-21206)
Goat anti-GFAP[4] (1:1000, Abcam, ab53554)	Normal Donkey Serum	Donkey anti-Goat, Alexa Fluor 488 (1:1000, Invitrogen, A-11055)
Goat anti-Iba1[4] (1:500, Abcam, ab107159)	Normal Donkey Serum	Donkey anti-Goat, Alexa Fluor 488 (1:1000, Invitrogen, A-11055)
Cleaved Caspase-3 (1:500, Cell Signaling technology, 9661s)	Normal Donkey Serum	Donkey anti-Rabbit, Alexa Fluor 488 (1:1000, Invitrogen, A-21206)